Journal of Hazardous Materials 168 (2009) 1004–1011

Contents lists available at ScienceDirect

Journal of Hazardous Materials

journal homepage: www.elsevier.com/locate/jhazmat

Removal of fluoride by hydrous manganese oxide-coated alumina: Performance and mechanism

Shao-Xiang Teng, Shu-Guang Wang*, Wen-Xin Gong, Xian-Wei Liu, Bao-Yu Gao

School of Environmental Science and Engineering, Shandong University, Jinan, 250100, China

ARTICLE INFO

Article history:
Received 16 July 2008
Received in revised form 11 February 2009
Accepted 24 February 2009
Available online 9 March 2009

Keywords:
Fluoride
Adsorption
Hydrous-manganese-oxide-coated alumina (HMOCA)
Ion-exchange
Column studies

ABSTRACT

A novel hydrous-manganese-oxide-coated alumina (HMOCA) material was prepared through a redox process. The adsorbent was characterized by SEM, BET surface area measurement, XRD, pH_{PZC} measurement, FTIR spectroscopy, and XPS. The manganese oxides were amorphous and manganese existed mainly in the +IV oxidation state. Batch and column experiments were carried out to investigate the adsorption potential of the adsorbent. Fluoride adsorption onto HMOCA followed the pseudo-second-order equation well with a correlation coefficient greater than 0.99. Both external and intraparticle diffusion contributed to the rate of transfer and removal. The adsorption of fluoride was thought to take place mainly by ion-exchange. Optimum removal of fluoride occurred in a pH range of 4.0–6.0. The maximum adsorption capacity calculated from the Langmuir model was 7.09 mg/g. The presence of HCO_3^-, SO_4^{2-} and PO_4^{3-} had negative effects on the adsorption of fluoride. The adsorbed fluoride can be released by alkali solution. Column studies were performed and 669 bed volumes were treated with the effluent fluoride under 1.0 mg/L at an influent F^- concentration of 5.0 mg/L and flow rate of 2.39 $m^3/(m^2\ h)$ (empty bed contact time = 7.5 min).

1. Introduction

Presence of fluoride in drinking water can be beneficial or harmful depending on its concentration. An appropriate concentration of fluoride (0.5–1.0 mg/L) is required to prevent dental cavities. However, excess ingestion of fluoride with high concentration can induce mottling of teeth, softening of bones, even neurological damages [1]. Many people from North Africa, China and India have been suffering from fluoride poisoning [2]. The World Health Organization has set a guidance value of 1.5 mg/L for fluoride in drinking water [3] and the Chinese standard for it is 1.0 mg/L.

Fluoride pollution of water may occur due to both natural reasons and human activity. Since fluoride is present in several minerals, it can be leached out by rainwater thereby allowing it to contaminate ground and surface water. On the other hand, fluoride can be found in wastewater from the fluoride chemical industry, as well as the semiconductor, metal processing, fertilizer, and glass-manufacturing industries [4,5]. Due to the harm of fluoride to mankind when it overshoots a suitable level, it is necessary to reduce and control the fluoride concentration in water systems.

The most commonly used methods for the defluoridation of water are adsorption [6,7], ion exchange [8], precipitation [9], and electrodialysis [10]. Among these methods, adsorption is the most widely used. A large number of materials have been studied as adsorbents, such as activated alumina [11], activated carbon [12], calcite [13], red mud [14], layered double hydroxides [15–17] and fibrous adsorbents [18]. Among these adsorbents, activated alumina (AA) seems to be widely used [19,20]. However, the main disadvantage of AA is its poor adsorption kinetics and narrow available pH range (5.0–6.0) [21,22].

In recent years, considerable amount of work has been done on developing adsorbents coated with other elements for defluoridation of water, e.g. zirconium-impregnated collagen fiber [23], aluminum-impregnated carbon [24], alum-impregnated activated alumina [25]. These surface coating showed promising results for fluoride removal. Manganese oxides, which have a large surface area, microporous structure, and high affinity for metal ions such as Pb, Cu, Cd, Zn, and UO_2^{2+} [26], were among these surface coating elements. Maliyekkal et al. [21] coated manganese oxide on alumina and successfully increased the maximum fluoride uptake capacity from 1.08 mg/g to 2.85 mg/g. The surface coating also decreased the equilibrium time from 10 h to 3 h. However, the synthesis process was so complex needing heated at 150 °C for 5 h and then 500 °C for 3 h. Hydrous manganese oxide (HMO), an amorphous manganese oxide which can be prepared by a relatively easy redox reaction, has been studied as discrete particles or coatings on other minerals [27–28]. Results showed that HMO has a large surface with significant microporosity. More importantly, coating of HMO increases the surface area of adsorbents and enhances the affinity towards

* Corresponding author. Tel.: +86 531 88362802; fax: +86 531 88364513.
E-mail addresses: tengshaoxiang@gmail.com (S.-X. Teng), wsg@sdu.edu.cn (S.-G. Wang).

0304-3894/$ – see front matter © 2009 Elsevier B.V. All rights reserved.
doi:10.1016/j.jhazmat.2009.02.133

Nomenclature

b	constant related to the energy or net enthalpy of adsorption (L/mg)
BDST	bed depth service time
C_0	initial fluoride concentration (mg/L)
C_b	effluent concentration at breakthrough (mg/L)
C_e	fluoride concentration at equilibrium (mg/L)
C_t	fluoride concentration at time t (mg/L)
h	bed depth of column (m)
k_1	first-order rate constant of adsorption (1/min)
k_2	second-order rate constant of adsorption (g/(mg min))
k_i	constant of intraparticle diffusion (g/(mg min$^{1/2}$))
K	rate of solute transfer from the fluid to solid (L/(mg h))
K_F	constant related to the adsorption capacity (mg/g)
m	mass of adsorbent (g)
n	constant indicative of the adsorption intensity of the adsorbent
N_0	adsorption capacity (mg/L)
q_e	amount of adsorbed fluoride at equilibrium (mg/g)
q_t	amount of adsorbed fluoride at any time t (mg/g)
Q_{max}	maximum adsorption capacity (mg/g)
u	linear flow rate (m/h)
V	volume of solution (L)

contaminants. However, adsorption of fluoride onto hydrous manganese oxide has not been reported.

Therefore, the main objective of this research was to prepare a novel adsorbent with high adsorption potential by coating hydrous manganese oxide onto alumina surface through an easy process. Adsorption kinetics and isotherms were conducted and modeled to investigate the adsorption behavior. Mechanisms involved in fluoride removal were explored by combining material characterization and adsorption performance.

2. Materials and methods

2.1. Synthesis of adsorbent

The activated alumina (AA, purity >92%) used in this study was obtained from FRIEND Chemical Plant, Jinan, China. AA was crushed in mortar and sieved by standard screens to get a certain particle size range of 0.45–0.90 mm. AA particles were then washed with deionized water and dried at 50 °C for 24 h. The dried AA was used as the base material for hydrous manganese oxide-coated alumina (HMOCA) preparation.

Manganese oxide was coated on the AA surface through a redox process: 10.00 g of AA was suspended in 50 mL of deionized water and the suspension was stirred at room temperature vigorously. 0.015 mol of Mn(II) acetate was added to this suspension. Then, 154 mL of a 0.065 mol/L $KMnO_4$ solution was added under continuous stirring at about 1000 rpm. The color of the solution turned to dark brown immediately, indicating the formation and precipitation of MnO_2 according to Eq. (1).

$$3Mn^{2+} + 2MnO_4^- + 2H_2O = 5MnO_2\downarrow + 4H^+ \quad (1)$$

Finally, the HMOCA particles were washed and dried at 50 °C for 24 h.

Except AA, all other chemicals used in this study were of analytical grade.

2.2. Material characterization

Micrography of the exterior surface of uncoated AA and HMOCA was obtained by scanning electron microscopy (S-520, Hitachi, Japan) under 28 kV. Surface areas of both AA and HMOCA were measured with nitrogen chemisorptions measurements with BET analysis (Quantachrome, USA). The crystalline structure of the adsorbent was characterized by X-ray diffraction (XRD) (D/MAX-rA, Rigaku, Japan) with Ni-filtered Cu Kα radiation. XRD was operated at 40 kV and 70 mA with a scanning speed of 7°/min from 10° to 80°. The XRD data were matched with standard JCPDS data. The samples of AA, HMOCA and HMOCA adsorbed with F^- were also analyzed by the Fourier transform infrared spectroscopy (FTIR) spectroscopy (Aratar, Thermo-NicoLet, USA) and the X-ray photoelectron spectroscopy (XPS) (PHI 5300, USA). For FTIR and XPS characterization, 0.25 g of HMOCA was added to 50 mL of fluoride solution with the concentration of 40 mg/L (high concentration was chosen to enhance the signal of F peak). After shaking for 4 h, the resulted HMOCA was dried and analyzed by FTIR and XPS. pH_{PZC} (pH of point of zero charge) of HMOCA was determined by batch equilibrium method [29]: HMOCA (0.25 g) was immersed in 50 mL 0.01 or 0.1 mol/L KNO_3 solution with different pH values, and shaken at 180 rpm for 24 h in capped bottles. KOH or HNO_3 solutions were used to adjust the initial pH values (3.0–12.0). Initial and final pH values were measured as pH_i and pH_f, respectively. pH_{PZC} was obtained as pH_f where common plateau was obtained.

2.3. Batch adsorption studies

A 100 mg/L fluoride stock solution was prepared by dissolving 0.2210 g of NaF in 1000 mL of deionized water. The test solution was prepared by diluting the stock solution to certain concentrations with deionized water. pH value for deionized water was 5.2 ± 0.05 and no pH adjustments were made except illustration. Adsorption experiments were performed by agitating 5.0 g/L of HMOCA with 50 mL of fluoride solution of desired concentrations at room temperature (about 25 °C) in different Teflon bottles capped tightly in a shaking machine operated at 180 rpm. At the end of predetermined time intervals, the concentration of fluoride was measured using a fluoride ion-selective electrode (PF-1, Shanghai Ruosull Technology LTD) after mixing with total ionic strength adjustment buffer (TISAB) according to the Methods of Examination of Water and Wastewater [30]. Experimental variables considered were: (1) contact time between adsorbent and the fluoride solution, 0–4 h; (2) initial concentrations of fluoride, 10–70 mg/L; (3) pH of solution, 3.0–12.0; and (4) coexisting ions, NO_3^-, Cl^-, HCO_3^-, SO_4^{2-}, PO_4^{3-} and fulvic acid (FA). Batch experiments were conducted thrice and average values were reported. Fluoride adsorbed by HMOCA was calculated by the following equation:

$$q_t = \frac{(C_0 - C_t)V}{m} \quad (2)$$

2.4. Desorption studies

HMOCA (0.25 g) were suspended in 50 mL of fluoride solution (6.0 mg/L), and the adsorption was conducted with constant shaking for 2 h at a pH of 5.2 ± 0.05. Then the solution was filtered and the adsorbent was transferred to 50 mL of deionized water with varying pH (3.0–13.5) adjusted with NaOH or HCl solutions. The solution was then shaken for 24 h after which fluoride concentration in the solution was analyzed.

Table 1
Textural properties of AA and HMOCA.

Sample	BET specific surface area (m^2/g)	Average pore width[a] (nm)	Pore volume[a] (cm^3/g)	Fractal dimension[b]
AA	297.1	5.086	0.391	1.4
HMOCA	315.5	5.086	0.407	2.4

[a] Obtained from density functional theory.
[b] Calculated using Frenkel–Halsey–Hill model.

2.5. Column studies

Column studies were carried out with columns ($H \times D$ = 50 cm × 2.4 cm). Each column was filled with 140 g of HMOCA and the bed height was 30 cm. Synthetic solution with known concentration of fluoride was fed to the top of the column at a desired flow rate continuously. Samples were collected at different bed heights and analyzed for the residual concentration of fluoride. The process was continued till concentration of the fluoride in the effluent reached the influent concentration, i.e., $C_t/C_0 \sim 1$. All the experiments were carried out at room temperature (about 25 °C) and no pH adjustments were conducted. The results obtained were plotted in terms of C_t/C_0 against bed volume (BV).

3. Results

3.1. Characterization of HMOCA

The samples of HMOCA were dark colored (brown–black) particles, indicating the presence of manganese in the form of insoluble oxides. Energy-dispersive analysis of X-rays (EDAX) showed the atom proportion of Al to Mn at the surface was about 3.2:1. The XRD of the samples (data not shown) did not show any peak, indicating the amorphous nature of the adsorbent.

Surface morphology of AA and HMOCA were shown in Fig. 1. Compared with virgin AA, HMOCA had a significantly rougher surface with lots of pores and the surface was apparently occupied by the newborn manganese oxides formed during the coating process. Textural properties obtained from nitrogen adsorption/desorption isotherms were summarized in Table 1. BET surface area of AA increased from 297.1 m^2/g to 315.5 m^2/g slightly after surface coating. The pH_{PZC} value for HMOCA was found to be 5.9.

FTIR spectrum of HMOCA showed major peaks at around 3400 cm^{-1} and 1636 cm^{-1} due to the stretching vibration of hydroxyl groups (–OH) and bending vibration of water molecules, respectively [31] (Fig. S1). After adsorption, the peak shift to 3420 cm^{-1} and decreased in intensity slightly, indicating the involvement of –OH in the fluoride adsorption.

XPS can be used to determine the surface structure and elemental composition of the near surface of solids. XPS analysis was performed on samples of AA, HMOCA and HMOCA reacting with fluoride. The wide scan of samples is presented in Fig. 2. It can be noticed that the major elements of HMOCA are Mn, O and Al. On the samples exposed to NaF, F peak was observed near 685 eV (Fig. 2c), indicating the adsorption of fluoride by the surface. Huang et al. [32] also found this F peak during their sol–gel–solvothermal processes.

Manganese oxides are generally expressed with the chemical formula of MnO_x, due to the multiple valence states exhibited by Mn. Two main peaks due to Mn 2p1 and Mn 2p3 were obtained at 654.13 eV and 642.46 eV, respectively. Binding energy of Mn 2p3 was usually used to identify the valence of manganese. The component at 642.46 eV can be attributed to Mn^{4+} [33]. After exposed to NaF, these Mn peaks moved to a higher energy side (643.17 eV, Mn^{4+} still). This may be caused by the interaction between fluoride and manganese.

3.2. Kinetic studies

Fig. 3 shows the time dependence of fluoride adsorption onto HMOCA at various initial concentrations. It has been observed that most of adsorption takes place within 30 min. After the initial 30 min, the rate of adsorption was negligible and the residual flu-

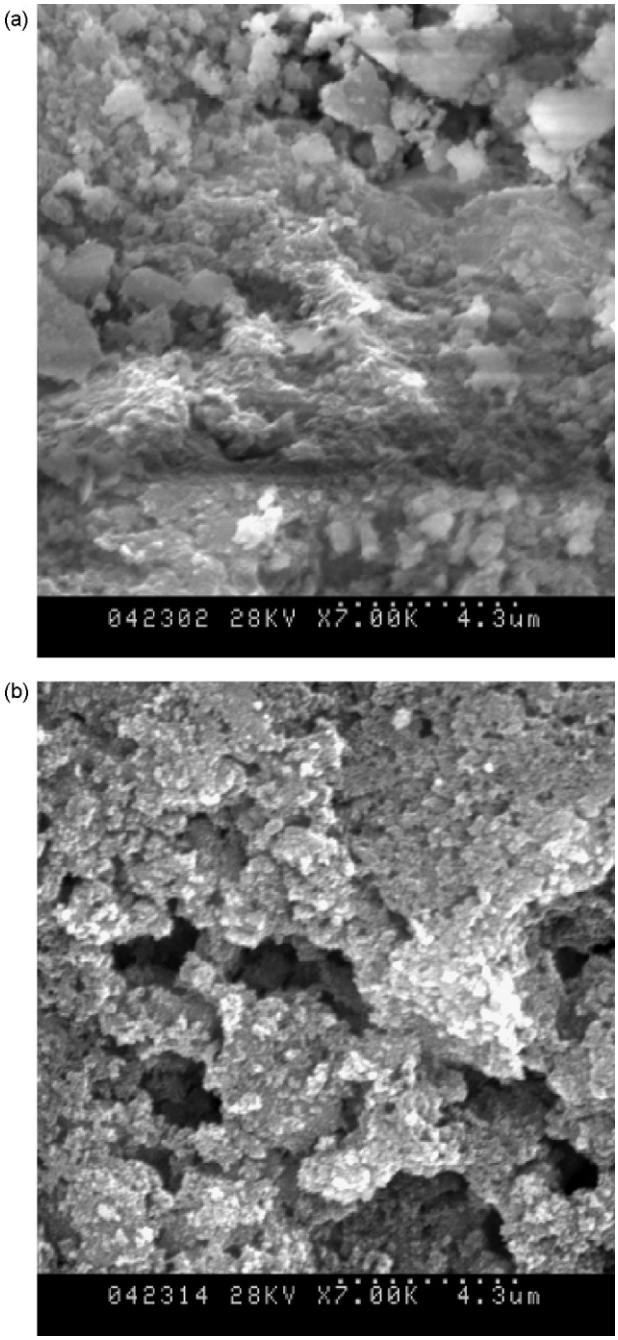

Fig. 1. SEM micrograph of samples: (a) AA; (b) HMOCA.

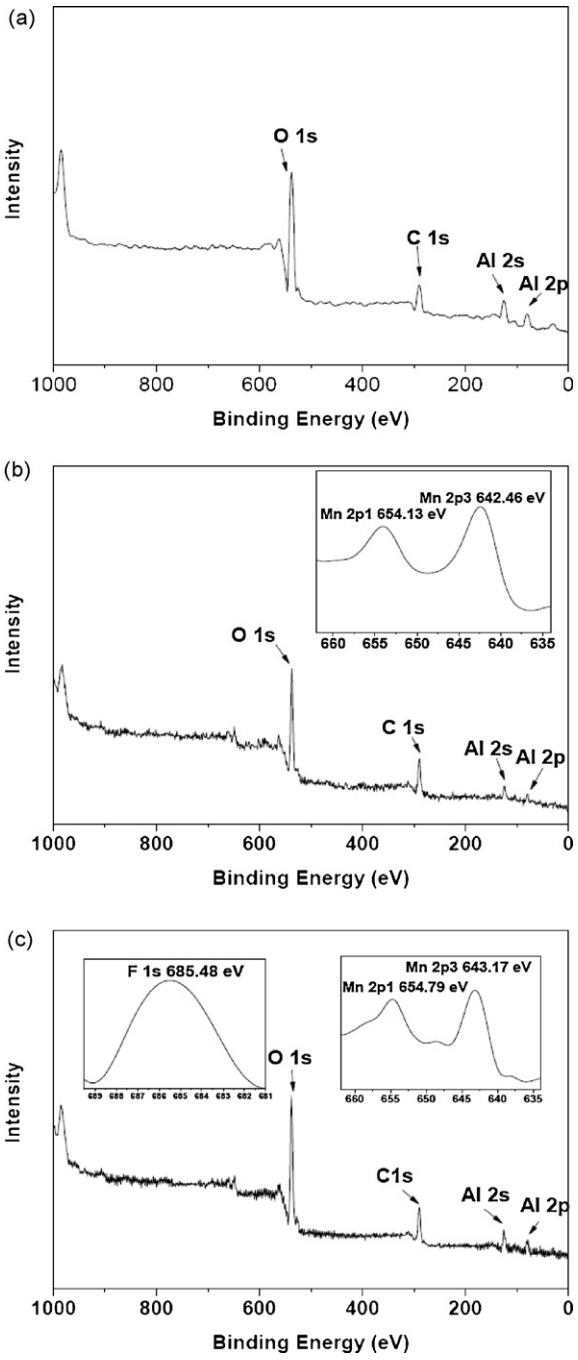

Fig. 2. XPS scan of samples: (a) AA; (b) HMOCA; (c) HMOCA after adsorption.

oride concentration in solution reached an almost constant value. The amount of fluoride adsorbed by HMOCA and time needed to reach equilibrium increased with the increasing initial fluoride concentrations.

The pseudo-first-order and the pseudo-second-order adsorption model were used to test adsorption kinetic data. The pseudo-first-order adsorption kinetic model is given as [34]:

$$\ln(q_e - q_t) = \ln q_e - k_1 t \quad (3)$$

The pseudo-second-order adsorption kinetic model is given as [35]:

$$\frac{t}{q_t} = \frac{1}{k_2 q_e^2} + \frac{1}{q_e} t \quad (4)$$

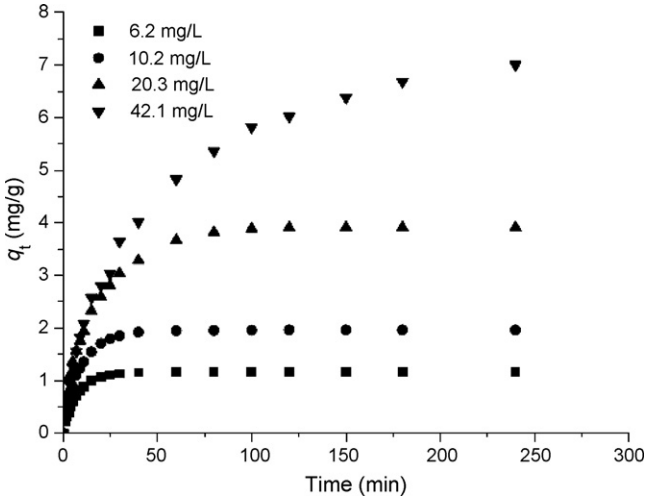

Fig. 3. Adsorption kinetic curves of fluoride at various initial fluoride concentrations (adsorbent dose = 5.0 g/L, pH = 5.2 ± 0.05, room temperature).

Kinetics constants obtained from the pseudo-first-order and second-order models are given in Table 2. Table 2 indicates that the kinetic data fit well with both the pseudo-first-order and pseudo-second-order kinetic models. The values of correlation coefficient R^2 for pseudo-first-order and pseudo-second-order kinetic models were relatively high (>0.99), and the adsorption capacities calculated by the models were also close to those obtained from experiments. The pseudo-first-order kinetic model indicates that the adsorption process occurs at a rate proportional to fluoride concentration. The well-fitting to pseudo-second-order kinetic model suggests a chemisorption process involving ion exchange [36].

The contribution of intraparticle diffusion to adsorption process can be described by Weber–Morris model. The rate of intraparticle diffusion is a function of $t^{0.5}$ and can be defined as follows [37]:

$$q_t = k_i t^{0.5} \quad (5)$$

where k_i can be obtained from the slope of the plot of q_t against $t^{0.5}$. The plot should be linear if intraparticle diffusion is involved in the adsorption process. Moreover, the line would pass through the origin if the intraparticle diffusion is the only rate-controlling step. However, if the line presents multi-linearity, it indicates the complexity of the adsorption process. The initial curved portion represents the boundary layer diffusion while the following linear portion attributes to intraparticle diffusion. The third plateau portion is the final equilibrium stage [38].

Fig. 4 shows the intraparticle diffusion plots for the adsorption of fluoride onto HMOCA. It could be seen that all plots had three portions attributed to boundary layer diffusion, intraparticle diffusion and equilibrium stage, respectively. The Weber–Morris model could describe the linear portion well ($R^2 > 0.99$), but the second linear portion did not pass through the origin. Therefore, it could be concluded that the adsorption process was complex and both external and intraparticle diffusion contributed to the rate of removal and transfer from the bulk phase to the solid surface. As can be seen form Fig. 4, the slopes and intercept of the plots increased with the increasing initial fluoride concentrations. The increased slope values (k_i) can be explained by the growing effect of concentration gradient as driving force. The growing values of intercept, which give an idea of the thickness of the boundary layer, indicate the noticeable effects of external mass transfer resistance.

Table 2
Kinetics constants for adsorption of fluoride onto HMOCA.

Initial concentration (mg/L)	Pseudo-first-order			Pesudo-second-order			Measured
	K_1 (min^{-1})	q_e (mg/g)	R^2	k_2 (g/mg min)	q_e (mg/g)	R^2	$q_{e,exp}$ (mg/g)
6.2	0.115	1.04	0.999	0.229	0.98	0.994	1.16
10.2	0.062	1.23	0.942	0.108	1.68	0.995	1.96
20.3	0.047	3.47	0.994	0.029	3.46	0.993	3.91
42.1	0.016	6.13	0.993	0.007	6.06	0.990	7.00

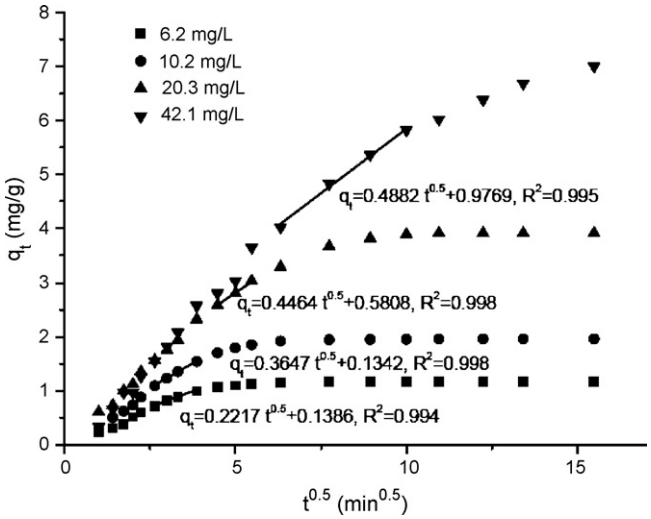

Fig. 4. Intraparticle diffusion plots for the adsorption of fluoride onto HMOCA at various initial concentrations (adsorbent dose = 5.0 g/L, pH = 5.2 ± 0.05, room temperature).

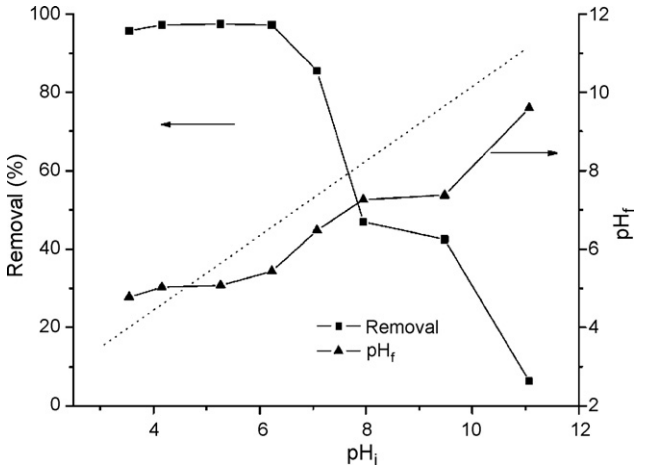

Fig. 5. Effect of pH on fluoride removal by HMOCA.

3.3. Equilibrium isotherms

Equilibrium studies were carried out at 30 °C with an initial pH of 5.2 ± 0.05 in order to determine the adsorption capacity of HMOCA. Langmuir and Freundlich isotherm models were used to fit the experimental data.

Langmuir model:

$$\frac{C_e}{q_e} = \frac{1}{Q_{max} b} + \frac{1}{Q_{max}} C_e \quad (6)$$

Freundlich model:

$$\ln q_e = \ln K_F + \frac{1}{n} \ln C_e \quad (7)$$

Table 3 gives the Freundlich and Langmuir isotherm constants.

It was clear that the Langmuir model gave a better fit to the experimental data than Freundlich isotherm with a correlation coefficient of 0.999. The maximum adsorption capacity of HMOCA calculated from Langmuir model was 7.09 mg/g, close to the value obtained from the experiments. These results suggested that the adsorption of fluoride on HMOCA involved the monolayer coverage of fluoride on the surface of the adsorbent.

Equilibrium parameter, R_L, defined as $1/(1 + bC_0)$ can be used to indicate the type of isotherm. R_L values calculated from the present system were presented in Table 3. R_L values were within 0 and 1 indicating a favorable adsorption process [39]. It seems that the adsorption was more favorable at higher concentrations.

3.4. Effect of solution pH

The effect of pH on removing fluoride from aqueous solution by HMOCA was studied at various pH (ranking from 3.0 to 12.0). The initial concentration of fluoride was maintained as 6.0 mg/L. Fig. 5 shows the effect of pH on fluoride adsorption onto HMOCA and the shifts in pH after adsorption. The results indicate that the optimum initial pH range of fluoride adsorption is 4.0–6.0 with removal efficiency higher than 95%. After that, the removal efficiency dramatically decreased and the adsorbent exhibited negligible adsorption (6.3%) at pH 11.1. The pH of the equilibrated solution increased under an initial acid pH range, while it decreased when the initial solution was alkaline. About 0.15 to 0.3 mg/L of Mn^{2+} was released to the final solutions when the pHs of initial solutions were ranked form 4 to 10. Release of Mn^{2+} was higher (>0.7 mg/L) at extreme pH conditions (pH < 4 and pH > 11) due to the simultaneous dissolution of Al_2O_3 under these situations.

3.5. Column studies

Synthetic fluoride solution with known concentration was fed to the top of the column at a desired flow rate. The breakthrough concentration for fluoride was 1.0 mg/L according to Chinese drinking water standard. Adsorbent was exhausted when fluoride in the effluent reached the influent concentration. Effects of flow rates,

Table 3
Freundlich and Langmuir isotherm constants for adsorption of fluoride onto HMOCA (initial fluoride concentrations 10–70 mg/L, pH = 5.2 ± 0.05).

T (°C)	Freundlich				Langmuir		
30	n	K_F (mg/g)	R^2		Q_{max} (mg/g)	b	R^2
	5.6	4.360	0.706		7.09	5.3	0.999
C_0 (mg/L)	10	20	30	40	50	60	70
R_L	0.018	0.0093	0.0062	0.0047	0.0037	0.0031	0.0027

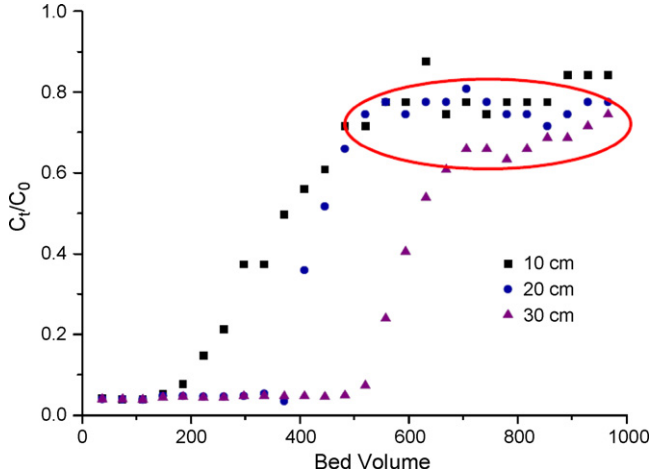

Fig. 6. Effect of bed depths on the breakthrough curve (initial concentration 5.0 mg/L, flow rate 2.39 $m^3/(m^2\,h)$, room temperature).

feed concentrations and bed depths on the breakthrough curves were investigated. The breakthrough point in the system occurred at about 669 BV, 610 BV and 557 BV for the flow rates of 2.39, 3.98 and 5.57 $m^3/(m^2\,h)$, respectively (Fig. S3). Sharper breakthrough curve was obtained at higher feed fluoride concentration. Fluoride concentration in the effluent overshot 1.0 mg/L at 120 BV when the feed concentration was 30.0 mg/L (Fig. S3).

In the bed depths experiment, 5.0 mg/L of fluoride solution was passed through the column at a fixed flow rate of 2.39 $m^3/(m^2\,h)$. Samples were collected at three different bed depths (10, 20 and 30 cm). The breakthrough curves are shown in Fig. 6. As it was evident from Fig. 6, an increase in column depth increased the treated volume due to longer contact time. At relatively shorter contact time, the breakthrough of the bed came earlier.

Bed depth service time (BDST) model fits well in the initial region of the breakthrough curve [40]. This model describes the relationship between the service time and the bed depth of the column. It could be expressed by the following equation [41]:

$$t = \frac{N_0}{uC_0}h - \frac{1}{KC_0}\ln\left(\frac{C_0}{C_b} - 1\right) \quad (9)$$

Eq. (9) enables the service time, t, of an adsorption bed to be determined for a specified bed depth, h, of adsorbent. The service time and bed depth are correlated with the process parameter such as initial pollutant concentration, solution flow rate and adsorption capacity. The plot of $t \sim h$ will be linear with a slope of N_0/uC_0 and an intercept of $(-1/KC_0)\ln(C_0/C_b - 1)$. C_b is 1.0 mg/L according to Chinese drinking water standard. The BDST model parameters can be used to predict the adsorption process with other operating conditions (different concentrations and flow rates) without further experiments.

Service times (corresponding to $C_t/C_0 = 0.2$ in Fig. 6) were found to be 14, 21, 29 h for 10, 20, 30 cm bed depths. The linear relationship obtained for fluoride adsorption onto HMOCA from the BDST plot for an initial concentration of 5.0 mg/L was given ($R^2 = 0.998$, Fig. S4):

$$t = 75h + 6.33 \quad (10)$$

The N_0 and K for HMOCA were calculated as 0.90 g/L and 0.044 L/(mg h), respectively.

The critical bed depth, h_c is obtained for $t = 0$ and for fixed outlet concentration $C_t = C_b$

$$h_c = \frac{V}{KN_0}\ln\left(\frac{C_0}{C_b} - 1\right) \quad (11)$$

h_c is the minimum bed depth necessary to get an effluent concentration C_b. The critical bed depth for fluoride obtained from BDST plot was 8.37 cm.

It was interesting to observe that the experimental results showed a plateau in the range of $C_t/C_0 = 0.6$–0.8.

4. Discussion

4.1. Coating of HMO on alumina

This study developed a simple and effective method to coat HMO on alumina surface. The new adsorbent could reduce fluoride concentration from 6.0 mg/L to 0.45 mg/L at an initial pH of 5.2 ± 0.05 while the removal efficiency was 45% for the virgin AA at the same condition. Chemical oxygen demand (COD) of the solution after adsorption was about 7 mg/L. About 0.2 mg/L manganese was released to the liquid in batch studies. According to Chinese drinking water standard, manganese should not overshoot 0.1 mg/L. But these released manganese cannot be detected in the effluent of column studies. No secondary pollution can be induced. The surface coating of manganese could be finished within several minutes, much easier than the method mentioned by Maliyekkal et al. [21]. Redox and precipitation were carried out at the same time. The redox and precipitation process should take responsibility for the amorphous structure of manganese oxide as it was unfavorable to the formation of micro-crystals [42]. After surface coating, virgin AA surface was occupied by manganese oxide and the surface became more porous (Fig. 1). BET analysis shows the surface area and pore volume were increased from 297.1 to 315.5 m^2/g and 0.391 to 0.407 mL/g, respectively. This slight increase maybe due to the new formed HMO [25]. Fractal dimension, a parameter reflecting the roughness of pore structure, increased from 1.4 to 2.4 after the formation of HMO, indicating a more irregular surface. Not all the surface coating processes increase surface areas. Pores may be covered due to the diffusion of coated particles [25]. As for MOCA prepared by Maliyekkal et al. [21], the surface area decreased after surface coating. The larger surface area and porous surface might contribute to the faster adsorption. Time needed to achieve equilibrium were 1 h, 3 h, and 10 h for HMOCA, MOCA and AA, respectively. A comparison has been made between HMOCA and previously reported adsorbents for fluoride removal based on three parameters (maximum adsorption capacity, particle size and pH range of high adsorption capacity) (Table 4). It seemed that the

Table 4
Comparison among various adsorbents used for fluoride removal.

Adsorbent	Adsorption capacity (mg/g)	Particle size	pH range of high adsorption capacity	References
AA	1.08	0.5–0.6 mm	5.0–6.0	[17]
MOCA	2.85	0.5–0.6 mm	5.0–7.0	[17]
Fe–Al–Ce trimetal oxide	178	Powder	5.5–7.0	[16]
MgAl–CO_3 layered double hydroxides	319.8	120 nm	5.0–7.0	[1]
Mixed rare earth oxides	196.08	4.34 μm	5.5–8.0	[4]
Red mud	6.29	<1 μm	4.0–6.0	[14]
Zn/Al hydrotalcite-like compound	13.43	Powder	6–7	[15]
HMOCA	7.09	0.45–0.90 mm	3.5–7.0	Present study

fine powder adsorbents had high adsorption capacities with the exception of red mud. However, fine powder could cause operational problems. Among the granular adsorbents, HMOCA had a larger adsorption capacity, and this adsorption capacity was sufficient for fluoride removal from ground water according to our study. Moreover, HMOCA showed a considerably high adsorption efficiency (>85%) over a relatively wide pH range of 3.5–7.0.

4.2. Mechanism of fluoride adsorption

Shifts of pH were observed during the experiments to identify the effect of solution pH as shown in Fig. 5. The pH of the equilibrated solution increased under an initial acid pH range, while it decreased when the initial solution was alkaline. The mechanism of fluoride removal by HMOCA was thought to be anion exchange between hydroxyl ion and F^- in the acid pH range. The increased pH after adsorption can be attributed to the liberation of OH^-. However anion-exchange was not favorable at pH > 6.0, fluoride was thought to be adsorbed by van der Waals forces at alkaline solution. When pH > 6.0, sodium ions were adsorbed while protons were released, leading to the decrease in final pH. Moreover, the surface of HMOCA tended to be electronegative when the initial pH > 6.0 since the pH_{PZC} of HMOCA was found to be 5.9. This would hold back the movement of F^- towards HMOCA surface due to the coulombic repulsion. Another reason for the decrease in adsorption in alkaline solution might be due to the strong competition between hydroxide ions and fluoride on active adsorption sites.

The most probable mechanism for fluoride removal by HMOCA at acid range can be described as follows [39,43,44]:

$$\mathrm{HMOCA{\cdot}}x\mathrm{H_2O_{(solid)}} + \mathrm{F_{(aq)}}^- \rightarrow \mathit{HMOCA}(x-1)\mathrm{H_2OH^+F_{(solid)}}^- + \mathit{OH}^- \quad (12)$$

This mechanism was likely to be favorable at pH < 6.0. However, at pH > 6.0, F^- might be adsorbed by following mechanism:

$$\mathrm{HMOCA{\cdot}}x\mathrm{H_2O_{(solid)}} + \mathrm{Na_{(aq)}}^+ + \mathrm{F_{(aq)}}^- \rightarrow \mathit{HMOCA}(x-1)\mathrm{H_2O{\cdot}OH^-Na^+F_{(solid)}}^- + \mathrm{H^+} \quad (13)$$

The FTIR results provide evidence for the involvement of –OH in fluoride adsorption. However, the changes in –OH peak was not very apparent. According to our calculation, adsorption capacity for the material used in FTIR characterization was about 7 mg F^-/g HMOCA. –OH involved in this fluoride adsorption may be not sufficient enough to induce obvious changes to the original broad and strong peak of hydroxyl group.

4.3. Adsorption and desorption

Kinetic studies of fluoride removal showed that both external and intraparticle diffusion contributed to the transfer rate from the bulk phase to the solid surface. The shaken conditions in the batch experiments increased the diffusion or transport of fluoride in the boundary layer and the internal surface of HMOCA. But during the column studies, mass transfer became much slower indicated by the breakthrough plateau in the range of C_t/C_0 = 0.6–0.8. Sperlich et al. [45] studied the breakthrough behavior of granular ferric hydroxide fixed-bed adsorption filters and their arsenate breakthrough curves also showed a non-ideal shape with a leveling off at $C_t/C_0 \sim 0.6$.

Based on batch and column studies of fluoride removal, intraparticle diffusion was a critical step in adsorption might due to the porosity of HMOCA. At the beginning of the column studies, a one-way non-cycle fluoride solution flowed through the HMOCA beds. There was nearly no residual fluoride (~0.2 mg/L) in the effluent due to the strong adsorption capacity of the fresh surface of HMOCA to F^-. With the adsorption sites occupied by fluoride, the effluent concentration increased sharply. Meanwhile, fluoride infiltrated to the interior of HMOCA gradually due to the porous surface of the adsorbent. The weakened surface adsorption and the enrichment of capillary concentration met balance, and residual fluoride concentration in effluent reached almost a constant value. When the HMOCA pores were filled to a certain degree, the capillary force weakened which resulted in the reduced fluoride absorption, then the HMOCA beds were exhausted totally [46].

Effects of coexisting ions (NO_3^-, Cl^-, HCO_3^-, SO_4^{2-}, PO_4^{3-} and FA) were studied (Fig. S5). It was found that NO_3^-, Cl^- (<300 mg/L) and FA (<30 mg/L) had negligible effect on the removal of fluoride. However, other common coexisting ions affected fluoride removal in the order of $PO_4^{3-} > SO_4^{2-} > HCO_3^-$. The fluoride removal efficiency was below 10% in the presence of 300 mg/L PO_4^{3-}.

Solutions at different pH were selected as the desorption reagents. Evidently, desorption efficiency of the solution varied with its pH value. Little fluoride was released at pH lower than 10.0. But desorption of fluoride took place as the pH increasing from 10.0 to 12.0 and reached maximum of 85% at pH 12.0 (Fig. S6). However, as the pH of solution increased further, AA and HMO coated on AA surface seemed to be detached which led to the decrease of the desorption efficiency. Although 85% of adsorbed fluoride could be recovered, the desorption process needed 24 h. The atom proportion of Al to Mn after desorption was about 6.5:1. R_L was used to indicate the type of isotherm. Adsorption process was irreversible when $R_L = 0$. R_L values calculated from our system were between 0 and 1 indicating a favorable adsorption, but the values were close to 0 (Table 3). This may be used to explain the difficulty of desorption. More effective desorption methods should be explored.

5. Conclusions

Hydrous manganese oxide was coated to the surface of AA to enhance fluoride removal potential in this study. HMOCA can reduce fluoride concentration from 6.0 mg/L to 0.45 mg/L while the removal efficiency was 45% for the virgin AA at the same condition. No secondary pollution was induced by organic or Mn^{2+} release. Adsorption kinetics followed the pseudo-second-order equation well. Adsorption isotherms can be well described by Langmuir equilibrium model. The maximum adsorption capacity was calculated to be 7.09 mg/g at pH 5.2 ± 0.05. Adsorption of fluoride was thought to take place mainly by ion-exchange. The optimum removal pH ranked from 4.0 to 6.0. Addition of HCO_3^-, SO_4^{2-} and PO_4^{3-} had negative effects on the adsorption of fluoride. Column study indicated practicality of HMOCA for fluoride removal from ground water.

Acknowledgements

The authors wish to thank the National Science and Technology Supporting Project (Grant No. 2006BAJ08B05-2) for the partial support of this study.

Appendix A. Supplementary data

Supplementary data associated with this article can be found, in the online version, at doi:10.1016/j.jhazmat.2009.02.133.

References

[1] X. Fan, D.J. Parker, M.D. Smith, Adsorption kinetics of fluoride on low cost materials, Water Res. 37 (2003) 4929–4937.
[2] J. Fawell, K. Bailey, J. Chilton, E. Dahi, L. Fewtrell, Y. Magara, Fluoride in Drinking-water, IWA/WHO, 2006.
[3] WHO, Chemical fact sheets: fluoride, in: Guidelines for drinking water quality (electronic resource): incorporation first addendum, Recommendations, vol. 1, third ed., Geneva, 2006, pp. 375–377.

[4] A.M. Raichur, M.J. Basu, Adsorption of fluoride onto mixed rare earth oxides, Sep. Purif. Technol. 24 (2001) 121–127.
[5] F. Shen, X.M. Chen, P. Gao, G.H. Chen, Electrochemical removal of fluoride ions from industrial wastewater, Chem. Eng. Sci. 58 (2003) 987–993.
[6] N. Azbar, A. Turkman, Defluoridation in drinking waters, Water Sci. Technol. 42 (2000) 403–407.
[7] E.J. Reardon, Y. Wang, Activation and regeneration of a soil sorbent for defluoridation of drinking water, Appl. Geochem. 16 (2001) 531–539.
[8] K. Vaaramaa, J. Lehto, Removal of metals and anions from drinking water by ion exchange, Desalination 155 (2003) 157–170.
[9] S. Saha, Treatment of aqueous effluent for fluoride removal, Water Res. 27 (1993) 1347–1350.
[10] Z. Amor, B. Bariou, N. Mameri, M. Taky, S. Nicolas, A. Elmidaou, Fluoride removal from brackish water by electrodialysis, Desalination 133 (2001) 215–223.
[11] S. Ghorai, K.K. Pant, Equilibrium, kinetics and breakthrough studies for adsorption of fluoride on activated alumina, Sep. Purif. Technol. 42 (2005) 265–271.
[12] Y.H. Li, S.G. Wang, X.F. Zhang, J.Q. Wei, C.L. Xu, Z.K. Luan, D.H. Wu, Adsorption of fluoride from water by aligned carbon nanotubes, Mater. Res. Bull. 38 (2003) 469–476.
[13] B.D. Turner, P. Binning, S.L.S. Stipp, Fluoride removal by calcite: evidence for fluorite precipitation and surface adsorption, Environ. Sci. Technol. 39 (2005) 9561–9568.
[14] Y. Çengeloğlu, E. Kır, M. Ersöz, Removal of fluoride from aqueous solution by using red mud, Sep. Purif. Technol. 28 (2002) 81–86.
[15] D.P. Das, J. Das, K. Parida, Physicochemical characterization and adsorption behavior of calcined Zn/Al hydrotalcite-like compound (HTlc) towards removal of fluoride from aqueous solution, J. Colloid Interface Sci. 261 (2003) 213–220.
[16] F. Delorme, A. Seron, A. Gautier, C. Crouzet, Comparison of the fluoride, arsenate and nitrate anions water depollution potential of a calcined quintinite, a layered double hydroxide compound, J. Mater. Sci. 42 (2007) 5799–5804.
[17] H.T. Wang, J. Chen, Y.F. Cai, J.F. Ji, L.W. Liu, H.H. Teng, Defluoridation of drinking water by Mg/Al hydrotalcite-like compounds and their calcined products, Appl. Clay Sci. 35 (2007) 59–66.
[18] R.X. Liu, J.L. Guo, H.X. Tang, Adsorption of fluoride, phosphate, and arsenate ions on a new type of ion exchange fiber, J. Colloid Interface Sci. 248 (2002) 268–274.
[19] N. Das, P. Pattanaik, R. Das, Defluoridation of drinking water using activated titanium rich bauxite, J. Colloid Interface Sci. 292 (2005) 1–10.
[20] X.M. Wu, Y. Zhang, X.M. Dou, M. Yang, Fluoride removal performance of a novel Fe–Al–Ce trimetal oxide adsorbent, Chemosphere 69 (2007) 1758–1764.
[21] S.M. Maliyekkal, A.K. Sharma, L. Philip, Manganese-oxide-coated alumina: a promising sorbent for defluoridation of water, Water Res. 40 (2006) 3497–3506.
[22] R.C. Meenakshi, Maheshwari, Fluoride in drinking water and its removal, J. Hazard. Mater. 137 (2006) 456–463.
[23] X.P. Liao, B. Shi, Adsorption of fluoride on zirconium (IV)-impregnated collagen fiber, Environ. Sci. Technol. 39 (2005) 4628–4632.
[24] R.L. Ramos, J.O. Turrubiarte, M.A.S. Castillo, Adsorption of fluoride from aqueous solution on aluminum-impregnated carbon, Carbon 37 (1999) 609–617.
[25] S.S. Tripathy, J.L. Bersillon, K. Gopal, Removal of fluoride from drinking water by adsorption onto alum-impregnated activated alumina, Sep. Purif. Technol. 50 (2006) 310–317.
[26] W.H. Zou, R.P. Han, Z.Z. Chen, J. Shi, H.M. Liu, Characterization and properties of manganese oxide coated zeolite as adsorbent for removal of copper (II) and lead (II) ions from solution, J. Chem. Eng. Data 51 (2006) 534–541.
[27] T. Boonfueng, L. Axe, Y. Xu, Properties and structure of manganese oxide-coated clay, J. Colloid Interface Sci. 281 (2005) 80–92.
[28] T. Boonfueng, L. Axe, Y. Xu, T.A. Tyson, Nickel and lead sequestration in manganese oxide-coated montmorillonite, J. Colloid Interface Sci. 303 (2006) 87–98.
[29] B.M. Babi, S.K. Milonjic, M.J. Polovina, B.V. Kaludierovic, Point of zero charge and intrinsic equilibrium constants of activated carbon cloth, Carbon 37 (1999) 477–481.
[30] F.S. Wei, Methods of Examination of Water and Wastewater, China Environmental Science Press, Beijing, 2002, pp. 189–193.
[31] S. Štandeker, Z. Novak, Ž. Knez, Adsorption of toxic organic compounds from water with hydrophobic silica aerogels, J. Colloid Interface Sci. 310 (2007) 362–368.
[32] D.G. Huang, S.J. Liao, J.M. Liu, Z. Dang, L. Petrik, Preparation of visible-light responsive N–F-codoped TiO_2 photocatalyst by a sol–gel-solvothermal method, J. Photochem. Photobiol. A 184 (2006) 282–288.
[33] T. Rao, M.Q. Shen, L.W. Jia, J.J. Hao, J. Wang, Oxidation of ethanol over Mn–Ce–O and Mn–Ce–Zr–O complex compounds synthesized by sol–gel method, Catalysis 8 (2007) 1743–1747.
[34] Y.S. Ho, G. McKay, The sorption of lead (II) ions on peat, Water Res. 33 (1999) 578–584.
[35] G. McKay, Y.S. Ho, Pseudo-second-order model for sorption processes, Process Biochem. 34 (1999) 451–465.
[36] Y.S. Ho, Review of second-order models for adsorption systems, J. Hazard. Mater. 136 (2006) (2006) 681–689.
[37] W.J. Weber, J.C. Morris, Kinetics of adsorption on carbon solution, J. Sanit. Eng. Div. Am. Soc. Civ. Eng. 89 (1963) 31–59.
[38] B.E. Wang, Y.Y. Hu, L. Xie, K. Peng, Biosorption behavior of azo dye by inactive CMC immobilized *Aspergillus fumigatus* beads, Bioresour. Technol. 99 (2008) 794–800.
[39] W. Nigussie, F. Zewge, B.S. Chandravanshi, Removal of excess fluoride from water using waste residue from alum manufacturing process, J. Hazard. Mater. 147 (2007) 954–963.
[40] T.S. Singh, K.K. Pant, Experimental and modelling studies on fixed bed adsorption of As(III) ions from aqueous solution, Sep. Purif. Technol. 48 (2006) 288–296.
[41] G.S. Bohart, E.Q. Adams, Behaviour of charcoal towards chlorine, J. Chem. Soc. 42 (1920) 523–529.
[42] J. Ma, X.J. Zhang, X.H. Cai, Y.C. Xie, Characterization of iron-manganese mixed oxides prepared by oxydoreduction precipitation method, J. Mol. Catal. (China) 13 (1999) 241–245.
[43] S. Dey, S. Goswami, U.C. Ghosh, Hydrous ferric oxide (HFO)—a scavenger for fluoride from contaminated water, Water Air Soil Pollut. 158 (2004) 311–323.
[44] A.A.M. Daifullah, S.M. Yakout, S.A. Elreefy, Adsorption of fluoride in aqueous solutions using $KMnO_4$-modified activated carbon derived from steam pyrolysis of rice straw, J. Hazard. Mater. 147 (2007) 633–643.
[45] A. Sperlich, A. Werner, A. Genz, G. Amy, E. Worch, M. Jekel, Breakthrough behavior of granular ferric hydroxide (GFH) fixed-bed adsorption filters: modeling and experimental approaches, Water Res. 39 (2005) 1190–1198.
[46] Z.G. Chen, C.B. Liu, Y. Zhang, T. Qiu, X. Liu, Dynamic adsorption of expanded graphite for oil in waste water of oil field, Mater. Mech. Eng. (China) 30 (2006) 81–83.